PCCP

Accepted Manuscript

ROYAL SOCIETY OF CHEMISTRY

www.rsc.org/pccp

Effect of oxygen and ozone on p-type doping of ultra-thin WSe_2 and $MoSe_2$ field effect transistors

Shunfeng Wang[1], Weijie Zhao[1], Francesco Giustiniano[1], Goki Eda[1,2,3,*]

[1] Department of Physics, National University of Singapore, 2 Science Drive 3, Singapore 117542

[2] Department of Chemistry, National University of Singapore, 3 Science Drive 3, Singapore 117543

[3] Centre for Advanced 2D Materials, National University of Singapore, 6 Science Drive 2, Singapore 117546

* Corresponding author: g.eda@nus.edu.sg

Abstract

We report on p-type doping effect of oxygen and ozone molecules on mono- and few-layer WSe_2 and $MoSe_2$ field effect transistors. We show that adsorption of oxygen and ozone in ambient conditions results in subtantial doping and corresponding enhancement in hole conductivity of the devices. Ozone-induced doping is found to be rapid and efficient, saturating within minutes of exposure whereas oxygen-induced doping occurs over a period of days to reach the equivalent level of doping. Our observations reveal that water adlayer on the material surface plays a crucial role in solubilizing oxygen and ozone and in forming a redox couple with a large chemical potential.

Introduction

Ultra-thin sheets of semiconducting transition metal dichalcogenides (TMDs) have been hailed as novel materials for next-generation electronics and optoelectronics[1]. Field-effect transistors (FETs) based on TMD layers exhibiting high field effect mobility and large on-off ratio have been demonstrated by a number of research groups[2-7]. The atomic thickness of these materials allow ultimate gate coupling and offer solution to short channel effects such as drain-induced barrier lowering and leakage current[8]. It is anticipated that these materials will enable realization of flexible and small-form-factor devices on a variety of surfaces [4, 9].

One of the fundamental challenges for the realization of TMD-based CMOS-type devices is controlled and reliable doping. It is imperative to establish a technique for achieving n-type and p-type doping in TMDs for their implementation into logic gates and diodes. It is known that cation substitution of group 6 TMDs such as MoS_2 with group 5 and group 7 elements leads to p-type and n-type doping, respectively [10]. However, substitutional doping is achieved only during crystal growth and with limited control over their concentration. Further, carrier mobility in substitutionally doped TMDs is significantly compromised due to ionized impurity scattering[11].

Charge transfer doping is a viable approach for modulating carrier concentration in two-dimensional (2D) semiconductors. Recent studies have shown that both n- and p-type doping can be induced by exposing 2D TMDs to oxidizing or reducing species with suitable redox potential[12-14]. For example, NH_3 and NO_2 can be used to dope MoS_2 n-type and p-type, respectively[15]. An adlayer of MoO_x having a large work function has also been shown to strongly dope 2D TMDs p-type[16, 17]. Doping by both physisorbed and chemisorbed species has been reported.[13]

While oxygen is recognized as a common adsorbate and an electron acceptor for carbon nanotubes and graphene[18, 19], its role on TMDs has not been systematically investigated. Here, we report the effects of oxygen and ozone on the transfer and output characteristics of mono- and few-layer WSe_2 and $MoSe_2$ FETs. We show that oxygen and ozone exposure result in metastable p-type doping and substantial increase in hole conductance. Our results demonstrate that while the doping mechanism is similar to that of ambient oxygen, ozone is a significantly more efficient electron acceptor owing its large redox potential. Further, we show that the presence of water adlayer that solubilizes the oxygen and ozone molecules is essential in invoking their powerful oxidizing properties.

Results and Discussion

Mono- and few-layer WSe_2 and $MoSe_2$ devices were fabricated following standard electron-beam lithography and electrode metal deposition. The electrical properties of the devices were then measured in a nitrogen-filled glove box. In typical fabrication procedures, the devices were annealed in the glovebox in order to drive off any residual adsorbates on the surface of the channel and improve metal-semiconductor contacts. In the following discussions, we refer to these annealed devices as "intrinsic" due to minimal surface adsorbates. The effect of surface adsorption of ambient oxygen on the device properties were studied by exposing the device to ambient air (relatively humidity of ~ 70%) for a fixed period time and subsequently measuring its transfer and output curves in nitrogen atmosphere. During ambient exposure, water is also expected to adsorb on the channel surface due to hygroscopic nature of TMDs.

As it will be discussed later, adsorption of water plays an important role in achieving significant doping. The effect of ozone on the device properties was studied by exposing the device to ozone in UV-ozone generator in the presence of ambient gas at room temperature (Fig 1a. See Methods for the details of ozone exposure). The level of ozone adsorption was controlled by varying the exposure time and the number of exposures.

Fig 1b shows changes in device conductance at V_g = -80 V as a function of progressive air and ozone exposure. Air-doping occurred gradually over a period of one week with a slow increase in device conductance by 3 orders of magnitude. In contrast, ozone led to immediate enhancement in device conductance by 3 orders of magnitude within the initial 11 minutes. Note that the enhancement achieved within 20 minutes of ozone exposure was larger than that achieved by air doping after one week. The general saturating trends are similar to those reported for air-doped graphene transistors.[18]

Fig 1c shows the transfer curve of a bilayer WSe_2 device in its intrinsic state while Fig 1d and e are those after exposure to ambient air for 12 hours, and after subsequent exposure to ozone for 11 min, respectively. Ambient air and ozone exposure resulted in progressive shift of the threshold voltage of both hole branch and electron branch to larger back gate voltages revealing increasing p-type character. Correspondingly, the maximum on-state current density increased from 1.6 μA/um to 15 μA/um by air exposure, and to 30 μA/um by ozone exposure, resulting in an increase in on-off ratio to above 10^7. Similar behaviors were observed for monolayer WSe_2 (Fig S1a), mono- and few-layer $MoSe_2$ (Fig S1b and c).

In order to verify that the above observations are due to an increase in hole concentrations, we studied the low temperature photoluminescence spectrum of the samples. The photoluminescence spectrum of monolayer WSe_2 at 77 K after air exposure for several days (Fig 2a) and after ozone treatment for 11 min (Fig 2b) reveals peaks arising from the neutral excitons and trions, or charged excitons, as expected for doped samples (See Supporting Information for a detailed spectrum). The separation between the twin peaks is 21 meV which is consistent with the binding energy of trions in WSe_2.[20] As can been seen, the trion-exciton intensity ratio for ozone-treated sample is larger than that for air-exposed sample, indicating higher hole density achieved with ozone treatment.

Similar to ambient gas doping of MoS_2[21], ozone doping was found to be a reversible process. Annealing ozone-treated devices in nitrogen atmosphere above 150 ^oC resulted in lower conductance of the original intrinsic state. Subsequent second exposure to ozone recovered the high doping state equivalent to that of the first exposure. As can be seen in Fig 3 and Fig S5, this doping and de-doping process can be repeated several times with high reproducibility, indicating no degradation of the material. These findings suggest that the doping is enabled by physisorption rather than chemisorption of ozone molecules.

The drastic enhancement in channel current upon exposure to ambient air and ozone can be attributed to changes in the contact resistance (R_c) and channel sheet resistance (ρ_{sh}). We investigated the changes in these contributions in devices using transfer length method (TLM). The total device resistance scales as $R_{tot}=2R_c+\rho_{sh}\cdot L/W$, where L is the channel length and W is the channel width. Thus the intercept and the slope of R_{tot}-L plot yields R_c and ρ_{sh}/W, respectively. We studied few-layer devices with channel lengths ranging from 1 to 5 μm (See Supporting Information for details of device fabrication). Fig 4a and b show R_{tot}-L plots for devices measured before and after ozone exposure. Both contact resistance (Fig 4c) and sheet

resistance (Fig 4d) at a given gate voltage shows a decrease by a factor more than 2 after exposure to ozone.

We evaluated the field effect mobility of the devices by $\mu = 1/C_{ox} \times [d\rho_{sh}^{-1}/dV_g]$, where C_{ox} is the oxide capacitance. The mobility of the device before and after exposure was found to be 98.7 $cm^2/V{\cdot}s$ and 99.3 $cm^2/V{\cdot}s$, respectively. The negligible change in mobility suggests that ozone adsorbates are not the dominant scattering centers in these systems. This observation is consistent with the non-covalent nature of ozone doping. Given that the mobility is not affected by ozone doping, the carrier density introduced by ozone can be estimated from the horizontal shift of ρ_{sh}-V_g plot (Fig 4d), which is found to be around 37 V. From the oxide capacitance, this shift corresponds to ozone-induced carrier density of 2.7×10^{12} cm^{-2}.

Reduction in contact resistance can also be explained by increase in hole density in the channel and corresponding shift in the Fermi level.The lowering of Fermi level causes narrowing of Schottky barrier and the depletion region (Fig 4f). Since carriers are mostly injected into the channel by thermally assisted tunneling[22], the tunnelling probability increases exponentially with decrease in barrier width. This is schematically shown in Fig 4. The relationship between contact resistance and carrier density is given by[23]

$$R_c \propto e^{-(\frac{4\pi}{h}\emptyset_B\sqrt{(\varepsilon m_p)/(qp)})} \quad (1)$$

where Φ_B is the Schottky barrier height , ε is the dielectric constant, m_p is the effective mass of holes and p is the hole density. Note that the contact resistance decreases with decreasing gate voltages for before and after ozone treatment. The $R_c - V_g$ plot in Fig 4c shows good agreement with Eq (1). This observation also indicates that thermionic emission is not a dominant carrier injection mechanism in these devices.

Lavesque et al.[18] showed that oxygen doping in graphene occurs via solvation of the molecules in water adlayer. Doping by ambient air was attributed to electron transfer from graphene to an O_2/H_2O redox couple such that

$$O_2(aq) + 4H^+ + 4e^-(graphene) \rightleftharpoons 2H_2O. \quad (2)$$

Similar observations have been reported for carbon nanotube FETs[19]. We thus hypothesize that a similar doping mechanism is at play in our air- and ozone-doped devices. To test this hypothesis, we investigated the role of water on doping in WSe_2 by exposing dehydrated device to oxygen and ozone. Dehydration of the device surface was achieved by placing the device in an air-filled and sealed quartz tube and annealing it at 150°C for half an hour. The device was then cooled in a temperature gradient in order to avoid recondensation of water vapor on to the device channel (Fig 5a). Note that the device prepared in this way is exposed to oxygen but in absence of significant water adlayer. The quartz tube containing the device after annealing was then loaded inside an ozone stripper. Since quartz is transparent to UV light, ozone is generated inside the quartz tube containing oxygen gas. The device was subsequently measured in nitrogen atmosphere without exposing it to ambient air. Two-probe transfer curves of a dehydrated bilayer WSe_2 device exposed to oxygen and ozone are shown in Fig 5b. Interestingly, no sign of significant doping was observed in these devices. These observations indicate that presence of water adlayer on the surface of WSe_2 is essential for doping by either oxygen or ozone, similar to the case of graphene. It is also worth noting that dehydrated devices often showed reduction of hole current after prolonged ozone exposure. In

fact this reduction in conductivity was irreversible suggesting that ozone tends to oxidize or etch WSe_2 in the absence of protective water adlayer as reported in a recent study[24].

With these experimental findings, we can now better understand the doping mechanism. In ambient conditions, physisorption of water on TMD surfaces and interfaces is ubiquitous[2 18 25]. In the case of ozone doping, this water adlayer solvates O_3 moelcules, establishing a redox reaction

$$O_3(aq) + 2H^+ + 2e^-(WSe_2) \rightleftharpoons O_2 + H_2O \quad (3)$$

Ozone is a strong oxidizing agent and its redox potential E_{redox} lies below the chemical potential or Fermi level of WSe_2, $E_{F,WSe2}$. Thus, electrons are withdrawn from WSe_2, reducing its chemical potential until equilibrium is reached (Fig 5c). Correspondingly, the hole density in WSe_2 increases, giving rise to enhanced hole conductivity.

Rapid doping of WSe_2 by ozone can be attributed to both its high oxidation potential and high solubility in water adlayer. According to the Nernst equation[18], the redox potential of a redox system can be estimated by

$$E_{\text{redox}} = \mu_{e(SHE)} + E^o_{redox} - \frac{\alpha k_B T}{n_e F}(log(c_{OX}) - 4pH). \quad (4)$$

Here, $\mu_{e(SHE)}$=4.44eV is the standard hydrogen electrode (SHE) potential relative to the vacuum level, E^o_{redox} is the standard electrode potential of the reaction versus SHE, α is chemical activity, $k_B T$ is the thermal energy, n_e is the number of electrons, F is the Faraday constant, and c_{ox} is the concentration of O_2 or O_3. The value of c_{ox} is dependent on the solubility of the oxidizing agent in water. At room temperature, the solubility of ozone in water is more than 10 times that of oxygen. Given the standard electron potential of ozone (~2.08 eV) and oxygen (~1.23 eV), the redox potential of ozone lies below that of O_2, ranging from -5.3 eV to -6.42 eV for a realistic acidity of water in air (~pH=6)[18] . On the other hand, the valence band maximum for monolayer WSe_2 is predicted be at -5.16 eV by first principle calculations[26]. Thus, electrons in WSe_2 have sufficient driving force to transfer to the redox system in both O_2 and O_3 based redox systems. The efficient ozone-induced doping can be explained in terms of its high large standard electrode potential and water solubility of ozone. Further, the ability of ozone to render SiO_2 surface more hydrophilic may also explain the efficient doping.

In summary, we report the role of oxygen and ozone on p-type doping of WSe_2 and $MoSe_2$ devices. Both molecules are shown to induce increase in hole density via a non-covalent charge transfer process, leading to significant increase in hole conductance. Doping occurs by solubilization of oxidizing molecules in water adlayer that is naturally present in devices exposed to ambient air and thereby forming a redox couple with a chemical potential higher than that of WSe_2 and $MoSe_2$. Due to the higher oxidation potential and water solubility, ozone is significantly more efficient in doping these materials compared to oxygen. Nevertheless, oxygen doping can be equally effective after prolonged exposure to ambient air. These findings indicate that care needs to be taken when evaluating intrinsic device performances due to significant extrinsic effects arising from ordinary surface adsorbates.

Acknowledgement

G.E. acknowledges National Research Foundation, Prime Minister's Office, Singapore for funding the research under NRF Research Fellowship (NRF-NRFF2011-02) and medium-sized centre programme.

Methods

Device fabrication WSe_2 and $MoSe_2$ flakes were mechanically exfoliated on top of a silicon substrate with a 300nm thick SiO_2 layer and subsequently identified under an optical microscope. Standard electron beam lithography techniques were used to define alignment marks and then draw electrode patterns, using 950 PMMA A5 as the resist. Afterwards, Cr/Pd/Au (2nm/20nm/30nm) was thermally evaporated in sequence as the electrodes. Palladium was used because it acts as a good hole injection contact.

Electrical characterization All electrical measurements were conducted at room temperature in nitrogen-filled glove box. Transfer characteristics curves were collected by Agilent parameter analyzer B1500A. Source-drain bias was fixed at 1V for all gate sweep measurement. Measurements on UV/ozone-treated devices were conducted 5~10 min following the procedure. Thus, effects of residual photoexcited carriers can be ignored.

Ozone treatment Ozone was produced by a UV/ozone procleaner (BioForce Nanoscience). The devices were loaded into the chamber and the UV light was switched on for 1 minute, after which they were kept in the chamber for 10 minutes. The UV irradiation time was deliberately set low to avoid oxidation. Slightly longer UV irradiation time (3 min) was used for the devices for TLM.

References

1. Q. H. Wang, K. Kalantar-Zadeh, A. Kis, J. N. Coleman and M. S. Strano, *Nat Nano*, 2012, **7**, 699-712.
2. RadisavljevicB, RadenovicA, BrivioJ, GiacomettiV and KisA, *Nat Nano*, 2011, **6**, 147-150.
3. B. W. Baugher, H. O. Churchill, Y. Yang and P. Jarillo-Herrero, *Nano letters*, 2013, **13**, 4212-4216.
4. X. Cui, G.-H. Lee, Y. D. Kim, G. Arefe, P. Y. Huang, C.-H. Lee, D. A. Chenet, X. Zhang, L. Wang, F. Ye, F. Pizzocchero, B. S. Jessen, K. Watanabe, T. Taniguchi, D. A. Muller, T. Low, P. Kim and J. Hone, *Nat Nano*, 2015, **10**, 534-540.
5. H. Fang, S. Chuang, T. C. Chang, K. Takei, T. Takahashi and A. Javey, *Nano letters*, 2012, **12**, 3788-3792.
6. W. Liu, J. Kang, D. Sarkar, Y. Khatami, D. Jena and K. Banerjee, *Nano letters*, 2013, **13**, 1983-1990.
7. S. S. Li, S. F. Wang, D. M. Tang, W. J. Zhao, H. L. Xu, L. Q. Chu, Y. Bando, D. Golberg and G. Eda, *Appl. Mater. Today*, 2015, **1**, 60-66.
8. H. Liu, A. T. Neal and P. D. D. Ye, *Acs Nano*, 2012, **6**, 8563-8569.

9. J. Pu, Y. Yomogida, K. K. Liu, L. J. Li, Y. Iwasa and T. Takenobu, *Nano letters*, 2012, **12**, 4013-4017.
10. K. Dolui, I. Rungger, C. Das Pemmaraju and S. Sanvito, *Phys Rev B*, 2013, **88**.
11. J. Suh, T. E. Park, D. Y. Lin, D. Y. Fu, J. Park, H. J. Jung, Y. B. Chen, C. Ko, C. Jang, Y. H. Sun, R. Sinclair, J. Chang, S. Tongay and J. Q. Wu, *Nano letters*, 2014, **14**, 6976-6982.
12. P. D. Zhao, D. Kiriya, A. Azcatl, C. X. Zhang, M. Tosun, Y. S. Liu, M. Hettick, J. S. Kang, S. McDonnell, K. C. Santosh, J. H. Guo, K. Cho, R. M. Wallace and A. Javey, *Acs Nano*, 2014, **8**, 10808-10814.
13. H. Schmidt, F. Giustiniano and G. Eda, *Chemical Society Reviews*, 2015.
14. B. Liu, L. Chen, G. Liu, A. N. Abbas, M. Fathi and C. Zhou, *Acs Nano*, 2014, **8**, 5304-5314.
15. B. Cho, M. G. Hahm, M. Choi, J. Yoon, A. R. Kim, Y. J. Lee, S. G. Park, J. D. Kwon, C. S. Kim, M. Song, Y. Jeong, K. S. Nam, S. Lee, T. J. Yoo, C. G. Kang, B. H. Lee, H. C. Ko, P. M. Ajayan and D. H. Kim, *Sci Rep-Uk*, 2015, **5**.
16. S. Chuang, C. Battaglia, A. Azcatl, S. McDonnell, J. S. Kang, X. T. Yin, M. Tosun, R. Kapadia, H. Fang, R. M. Wallace and A. Javey, *Nano letters*, 2014, **14**, 1337-1342.
17. C. Han, J. D. Lin, D. Xiang, C. C. Wang, L. Wang and W. Chen, *Appl Phys Lett*, 2013, **103**.
18. P. L. Levesque, S. S. Sabri, C. M. Aguirre, J. Guillemette, M. Siaj, P. Desjardins, T. Szkopek and R. Martel, *Nano letters*, 2011, **11**, 132-137.
19. C. M. Aguirre, P. L. Levesque, M. Paillet, F. Lapointe, B. C. St-Antoine, P. Desjardins and R. Martel, *Adv Mater*, 2009, **21**, 3087-+.
20. A. M. Jones, H. Y. Yu, N. J. Ghimire, S. F. Wu, G. Aivazian, J. S. Ross, B. Zhao, J. Q. Yan, D. G. Mandrus, D. Xiao, W. Yao and X. D. Xu, *Nat Nanotechnol*, 2013, **8**, 634-638.
21. H. Schmidt, S. F. Wang, L. Q. Chu, M. Toh, R. Kumar, W. J. Zhao, A. H. C. Neto, J. Martin, S. Adam, B. Ozyilmaz and G. Eda, *Nano letters*, 2014, **14**, 1909-1913.
22. S. Das, H. Y. Chen, A. V. Penumatcha and J. Appenzeller, *Nano letters*, 2013, **13**, 100-105.
23. C. Hu, *Modern semiconductor devices for integrated circuits*, Prentice Hall, Upper Saddle River, N.J., 2010.
24. M. Yamamoto, S. Dutta, S. Aikawa, S. Nakaharai, K. Wakabayashi, M. S. Fuhrer, K. Ueno and K. Tsukagoshi, *Nano letters*, 2015, **15**, 2067-2073.
25. H. Qiu, L. J. Pan, Z. N. Yao, J. J. Li, Y. Shi and X. R. Wang, *Appl Phys Lett*, 2012, **100**.
26. J. Kang, S. Tongay, J. Zhou, J. B. Li and J. Q. Wu, *Appl Phys Lett*, 2013, **102**.

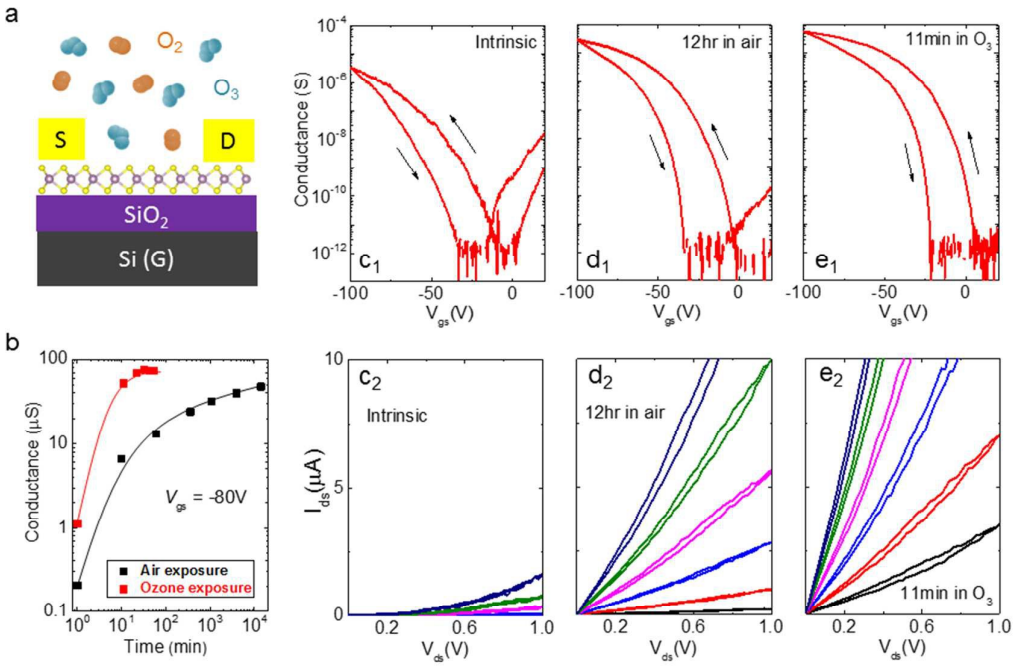

Figure 1. (a) Schematic diagram of WSe_2 transistor exposed to a mixture of oxygen and ozone molecules. (b) Conductance of a bilayer WSe_2 device at V_g = -80 V as a function of air and ozone exposure time. (c-e) Transfer (upper panels) and output (lower panels) curves of a bilayer WSe_2 device in its intrinsic state (c), after air exposure for 12 hours (d), and after subsequent ozone exposure for 11 minutes (e).

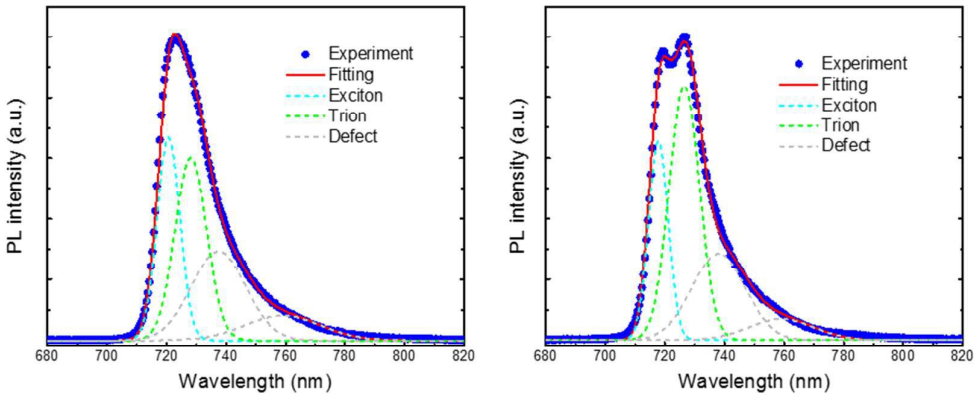

Figure 2. Photoluminescence (PL) of monolayer WSe_2 after air exposure for several days (a) and after subsequent ozone exposure for 11 mins (b). The spectra were fitted with exciton, trion and localized states emission peaks. The spectra were obtained in nitrogen atmosphere at liquid nitrogen temperature (77K).

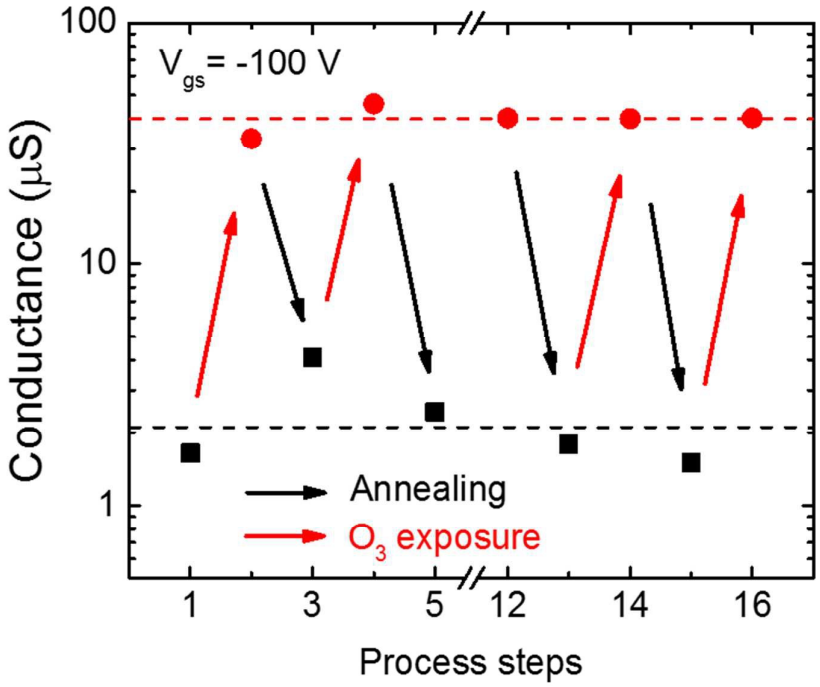

Figure 3. On-state conductance of a bilayer device at V_g = -100 V after exposure to ozone and annealing over multiple cycles. The device shows consistent undoped and doped conductance of ~2 μS and ~40 μS, respectively.

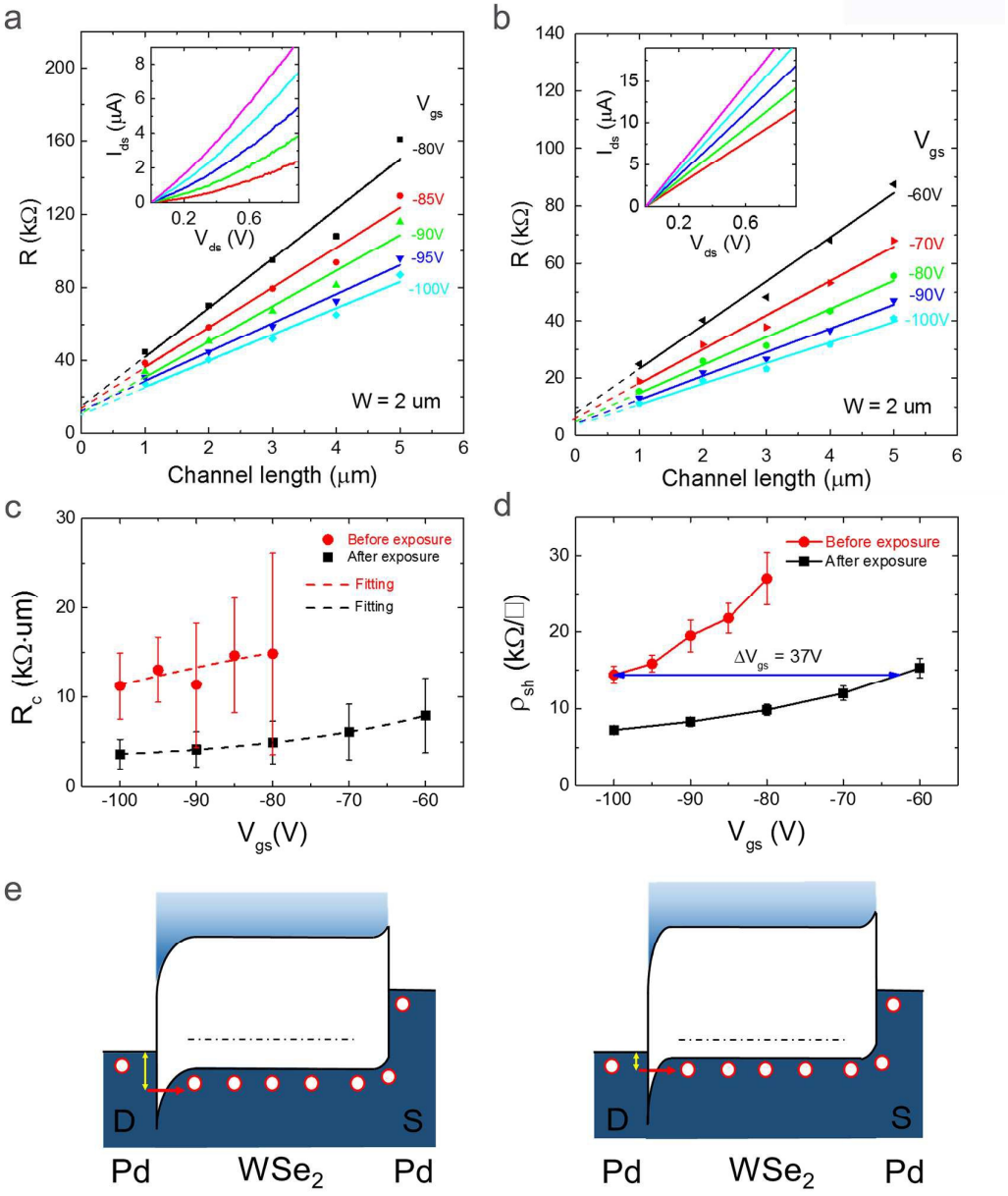

Figure 4. (a,b) Total resistance of multilayer WSe_2 devices as a function of channel length at different gate voltages before (a) and after (b) ozone exposure. The insets show output curves at gate voltages ranging between -60 and -100 V in 10 V steps. (c,d) Extracted values of (c) R_c and (d) ρ_{sh} as a function of gate voltages for deivces before and after ozone exposure. The dashed line in (c) is a fit according to Eq (1). (e) Schematic band diagram of WSe_2 transistor with Pd source and drain contacts. The dashed line indicates the Fermi level (E_F). In a weakly doped device, current injection is limited by the Schottky barrier at the contact. After doping, the Schottky barrier becomes narrower and thermionic tunneling of holes is facilitated.

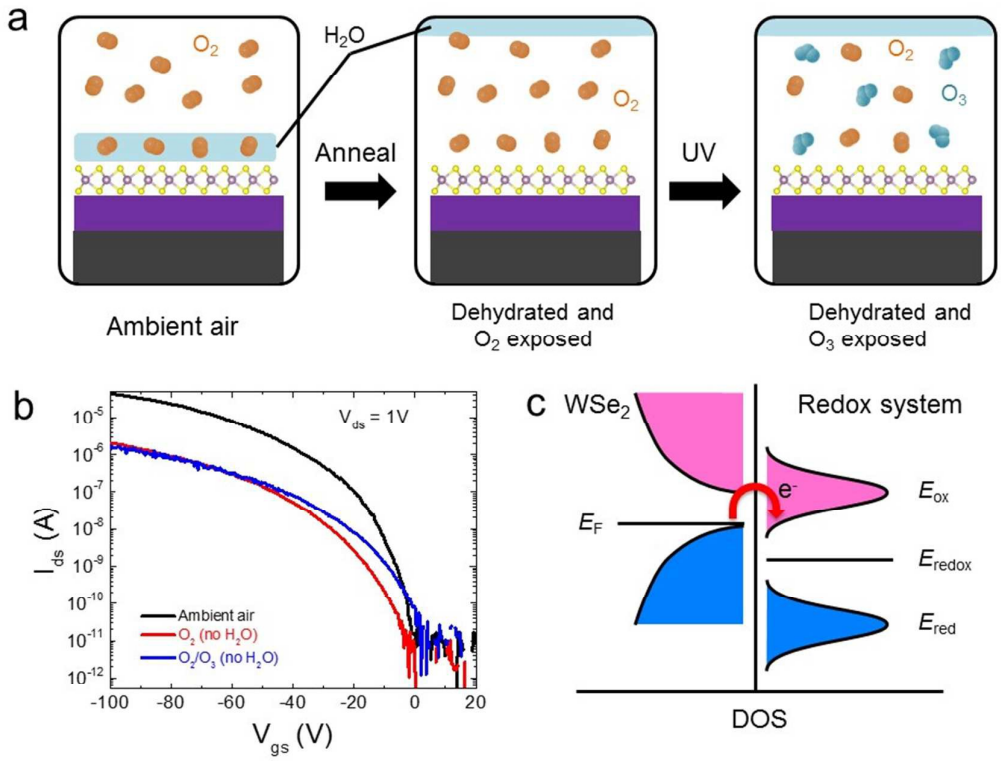

Fig 5. (a) Schematic showing the scheme for studying the role of water in oxygen and ozone doping. The water adlayer was removed by annealing the device enclsed in a quartz tube and cooling it over a temperature gradient to condense moisture on the inner walls of the quartz . Ozone is subsquently introduced by UV light exposure. (b) Transfer characteristics of the device in the conditions as illustrated in (a). (c) Schematic energy diagram showing the DOS of WSe_2 (left) relative to that of O_3/H_2O (or O_2/H_2O) redox system (right). Electrons transfer from WSe_2 to the redox system driven by the difference in E_F and E_{redox}.